Viable substrates for the honeycomb-borophene growth

Ze Yu [1,2] Sheng Meng,[1,2,4,*] and Miao Liu [1,3,4,†]

[1]*Beijing National Laboratory for Condensed Matter Physics and Institute of Physics,*
Chinese Academy of Sciences, Beijing 100190, China
[2]*School of Physical Sciences, University of Chinese Academy of Sciences, Beijing 100190, China*
[3]*Center of Materials Science and Optoelectronics Engineering, University of Chinese Academy of Sciences,*
Beijing 100049, People's Republic of China
[4]*Songshan Lake Materials Laboratory, Dongguan, Guangdong 523808, People's Republic of China*

The two-dimensional honeycomb lattice is an important system for investigating exotic quantum physics. Boron, the neighboring element of carbon, may form a flat monolayer honeycomb lattice, namely the honeycomb-borophene (*h*-B), on the surface of specific materials. In this work, we evaluate the potential of eight fcc metal materials, including fcc Ge, Nb, Ta, Ag, Ti, W, Al, and Mo, as the possible substrate for epitaxial *h*-B growth through the first-principles calculations. We find that Al(111) is one of the good candidates, while other fcc(111) surfaces of Nb, Ta, Ti, W, and Mo are also very likely to serve as viable substrates to support the *h*-B growth, since their film-substrate binding energies are even larger than that on Al(111). It has been identified that there is a strong charge accumulation effect between *h*-B and the metal substrate to stabilize the plane *h*-B. Combining the analysis from the thermodynamical and the electronic aspects, it is likely that the fcc phase of the Ta and W, other than Al, can serve as the best substrates for *h*-B growth, owing to their large adhesive energy (E_{ad}) and strong charge-transferring effect between *h*-B and substrate. However, it is nearly impossible to obtain a freestanding *h*-B for the same reason.

I. INTRODUCTION

Honeycomb lattice serves as a feasible model system to study massless Dirac fermions. Some of the exotic quantum states, such as the quantum Hall effect [1,2], quantum spin Hall effect [3–7], and quantum anomalous Hall effect [8,9] can be obtained within the honeycomb lattice when the electron hopping parameters or spin-orbit coupling are purposedly tuned within a certain region. If the in-plane σ bond of a honeycomb lattice, stabilized by strong electron-phonon interactions, is pinned to the Fermi level, the residual electron-phonon interactions can be strong enough to yield superconductivity [10,11]. Despite the rich physics in the honeycomb lattice, the likelihood to experimentally obtain the planar honeycomb lattice in solids is low, let alone a monolayer of honeycomb lattice on the surface of materials. Hence, the quantum physics research somewhat hinges on whether the planar honeycomb lattices can be made experimentally.

Graphene is the only flat and freestanding honeycomb lattice that can be synthesized experimentally [12] by far. Researchers have endeavored to extend this category of materials to other noncarbon elements such as boron [13–15], silicon [16–18], germanium [19], and phosphorus to search for graphenelike lattices. Boron is an adjacent element of carbon and has one electron less than carbon; as such, the

honeycomb boron layer is likely to exist on the surface if the system is electronically doped at a high doping level to allow the formation of the π bond. In fact, for the same reason, the honeycomb boron layers can be found in the bulk MgB_2 [10]. The low-dimensional boron allotropes, such as fullerenes [20,21] and boron nanotubes [22], have been found to share the same structure with carbon systems. However, from the thermodynamic point of view, the two-dimensional (2D) boron sheet (BS) has a rich family of low-dimensional allotropes such as $Pmmn$-B_8-sheet [15], α sheet [13], β_{12} sheet [23], and γ-B_{28} sheet [24], all competing with the formation of honeycomb-borophene (*h*-B). Therefore, it is a challenge to synthesize *h*-B in the real world.

Efforts have been made to gauge the synthesizability of the *h*-B. For example, Liu *et al.* [25] recommended that the 2D BS can be synthesized on metal substrates or metal boride. Liu *et al.* [26] explored the stability and growth mechanism of various BSs on Cu(111) substrates, and found that hexagonal holes can easily occur at the edge of the triangular boron cluster. Zhang *et al.* [27] studied monolayer boron adsorbed on substrates such as Mg and Al, and found that *h*-B is more energetically favorable than triangular boron sheets (*t*-BSs) or mixed hexagonal-triangular boron sheets (*ht*-BSs). In 2018, Li *et al.* [28] successfully synthesized the planar *h*-B by molecular-beam epitaxy (MBE) when employing Al(111) as the substrate, which is a milestone in the field of *h*-B synthesis.

As shown from this chain of research efforts on the synthesis of *h*-B, it indicates that finding a proper substrate that can accommodate the *h*-B growth is critical. Therefore, several

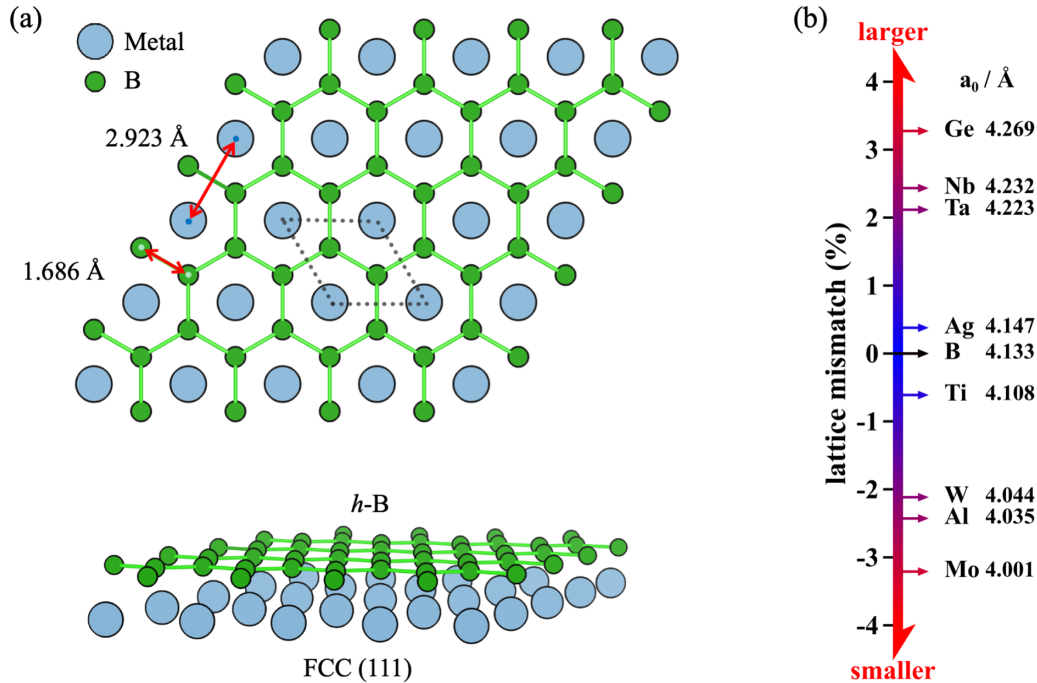*smeng@iphy.ac.cn
†mliu@iphy.ac.cn

104003-1

FIG. 1. The *h*-B and lattice mismatch of the metals. (a) Freestanding flat *h*-B and the (111) surface of ideal fcc metal. The red arrows indicate the B–B bond lengths and the intermetal distance of the ideal metal. (b) Lattice mismatch within 4%, where the number next to the chemical symbol is the corresponding lattice constant. The label "B" represents an ideal metal with a 0% lattice mismatch.

relevant questions are raised: (1) Are there good substrates, other than Al, that can host the *h*-B growth? (2) How does the substrate affect the growth of the *h*-B thermodynamically and electronically? (3) How strong or weak is the substrate-film binding? Is the *h*-B exfoliable? To answer these questions, we carried out the theoretical research focusing on investigating viable substrates that can enable the growth of *h*-B besides Al. Eight candidate substrates, mostly the face-centered cubic (fcc) metal phases, were evaluated via *ab initio* calculations. The result showed that *h*-B tends to chemically bind onto the metal substrate to ensure the formation of planar *h*-B, and the larger the adhesive energy, the more likely the planar *h*-B to exist. We predict that the fcc phase of the Ta and W can serve as the best substrates for *h*-B growth, which is better than Al. Their larger adhesive energy can make *h*-B more stable but their strong charge-transferring effect between *h*-B and substrate makes it nearly impossible to obtain freestanding *h*-B.

II. CALCULATION DETAILS

The first-principles calculations, which are based on density-functional theory (DFT) as implemented in the Vienna *Ab initio* Simulation Package (VASP), were employed throughout this work to model the material systems [29]. The Perdew-Burke-Ernzerhof [30] flavor of pseudopotential is selected to describe the exchange and correlation functions of the system within the generalized gradient approximation framework. The pseudopotentials are generated using the projector-augmented wave [31] method as provided along with the VASP code. The energy cutoff for plane-wave basis sets was set to be a fixed value of 450 eV for all calculations. We first relax the fcc phase of the metals (Ge, Nb, Ta, Ag,

Ti, W, Al, and Mo) to 1×10^{-6} eV for energy convergence and 0.01 eV/Å for force convergence. To simulate the film on metal substrates, the previously optimized fcc bulk phase with eight-layers metal atoms was expanded to a 3×3 super-cell. The vacuum thickness is always larger than 15 Å for all the slab calculations. We choose the (111) facet for the metal substrate termination as the (111) is the most stable surface for fcc metal and the hexagonal arrangement of atoms matches well with the honeycomb lattices. For the surface calculations, we fixed the bottom six layers of the substrate to mimic the thick substrate in the real world. The DFT-D3 treatment [32,33] is used to take the van der Waals interaction between the substrate and the film into account. The structural relaxation of energy and force convergence criteria are 1×10^{-5} eV and 0.05 eV/Å, respectively. The *k*-point mesh of $5 \times 5 \times 1$ is employed for the integral over the Brillouin zone. Meanwhile, the dipole correction [34] is incorporated to eliminate the effects of the artificial electric field. For all the calculations, spin polarized is considered when the volume magnetic susceptibility of metal is greater than 1×10^{-4}. In the molecular-dynamics calculations, we released all the substrate atoms and performed simulations at 300 K under the canonical (NVT) ensemble.

III. RESULTS AND DISCUSSION

The *h*-B (space group *P*6/*mmm*, No. 191) has threefold symmetry; hence, one of the most suitable metal substrates that can accommodate the *h*-B growth should be the (111) surface of fcc metal. To get a stable *h*-B, the best-case scenario is that the *h*-B is epitaxially grown on a metal substrate with a perfectly matched lattice to minimize the strain energy. The
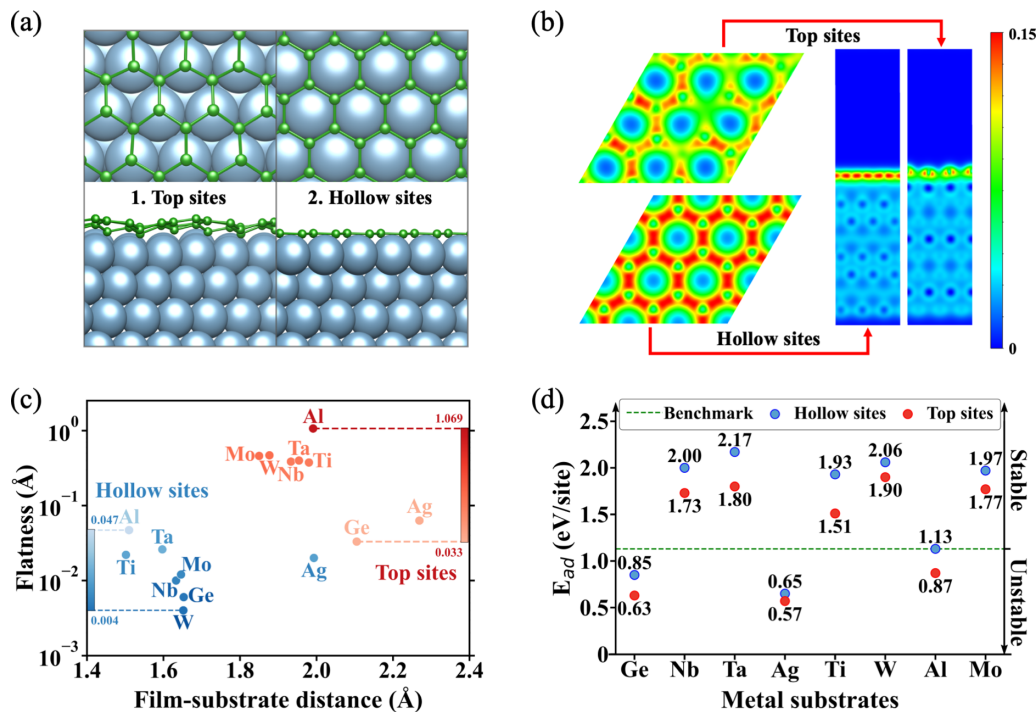
FIG. 2. Schematic structures, charge densities, geometric information, and E_{ad}. (a), (b) Top and side views of h-B and charge densities at the top sites and hollow sites of substrate Al. (c) The flatness of the h-B at the hollow and top sites, as a function of the distance between the h-B and the metal substrate. (d) The E_{ad} of h-B grown at the top and hollow sites of the eight substrates. The E_{ad} of the h-B grown at the hollow sites of Al was used as a comparative benchmark for stability.

B–B bond length of the monolayer freestanding flat h-B is 1.686 Å from our calculation, which implies the lattice constant that fits well the h-B is 4.133 Å for the conventional cell of fcc metals [Fig. 1(a)].

The B–B bond is, in most cases, stiffer than metal bonds. Therefore, a strain greater than 4% would rapidly increase the strain energy of the h-B and the system would be thermodynamically unstable. Filter all the possible elementary metals (within 40 candidates), 8 of which include Ge, Nb, Ta, Ag, Ti, W, Al, and Mo in the fcc phase fall out as the viable candidate substrates that can match the h-B geometrically [lattice mismatch <4%, Fig. 1(b)]. It is worth noting that, among the eight candidates, Ag and Al are stable in the fcc phase, and they have been experimentally evaluated in previous studies. As mentioned above, Al is by far the only substrate that capable of hosting the h-B via MBE synthesis [28]. Ag, although the lattice mismatch is small, yields the BSs (like γ-B$_{28}$) sheet instead of h-B [35]. Other candidate substrates, i.e., Ge, Nb, Ta, Ti, W, and Mo, are not fcc metals, but their fcc metastable phases may exist as thin films and hence are worth assessing.

DFT calculations are performed to get an idea on whether the h-B can grow on the metal substrates. It is possible that B atoms can stay on either top or hollow sites on fcc (111) surfaces; hence, both the sites are evaluated for all 8 substrates, totaling 16 cases. While the h-B may grow on both the top and hollow sites on fcc metal, they are not necessarily flat on these substrates. Figure 2(a) shows that the h-B is fairly planar at the hollow sites of the Al; however, it is buckling at the top sites of the Al with a concomitant inhomogeneous charge distribution [Fig. 2(b)].

As shown in Fig. 2(c), the flatness of h-B, defined as the maximum variance of the boron atom position along the c axis, is shown as a function of the film-substrate distance, which represents the binding strength between film and substrate to some extent. It is obvious that the film-substrate distance for the hollow sites is smaller than that of the top sites as the B atom stays in the "valley." The hollow sites tend to create better flatness for h-B growth, and the roughness of h-B at the hollow sites (0.004–0.047 Å) is at least one order of magnitude smaller than that at the top sites (0.033–1.069 Å). Therefore, the top sites might not be a good choice for growing flat h-B comparing to the hollow sites.

The film-substrate spacing at the hollow sites is 1.65, 1.63, 1.60, 1.99, 1.50, 1.65, 1.51, and 1.65 Å for Ge, Nb, Ta, Ag, Ti, W, Al, and Mo, respectively. The layer spacing of 1.54 Å given by Zhu *et al.* [36], for h-B growth on Al, is almost identical to ours. The layer spacing is correlated with structural stability and the exfoliation difficulty to a certain degree. The h-B on Al, although synthesizable, the small film-substrate spacing evidences a strong binding effect, suggesting it is unlikely to exfoliate the film from the surface. Overall, the value of film-substrate from the calculation exhibits that the h-B tends to chemically, rather than physically, bind onto the metal substrate, and the strong chemical bonding leads to flat h-B. Hence, it is unlikely to have a freestanding h-B in a 2D planar geometry; at least the chemistry or electronic structure of h-B prevents it from happening [13,22,37].

The adhesive energy, which is the energy cost to peel the film off from the substrate, is [$E_{ad} = (E_{\text{subtrate}} + E_{\text{film}} - E_{\text{total}})/N$]. The larger the adhesive
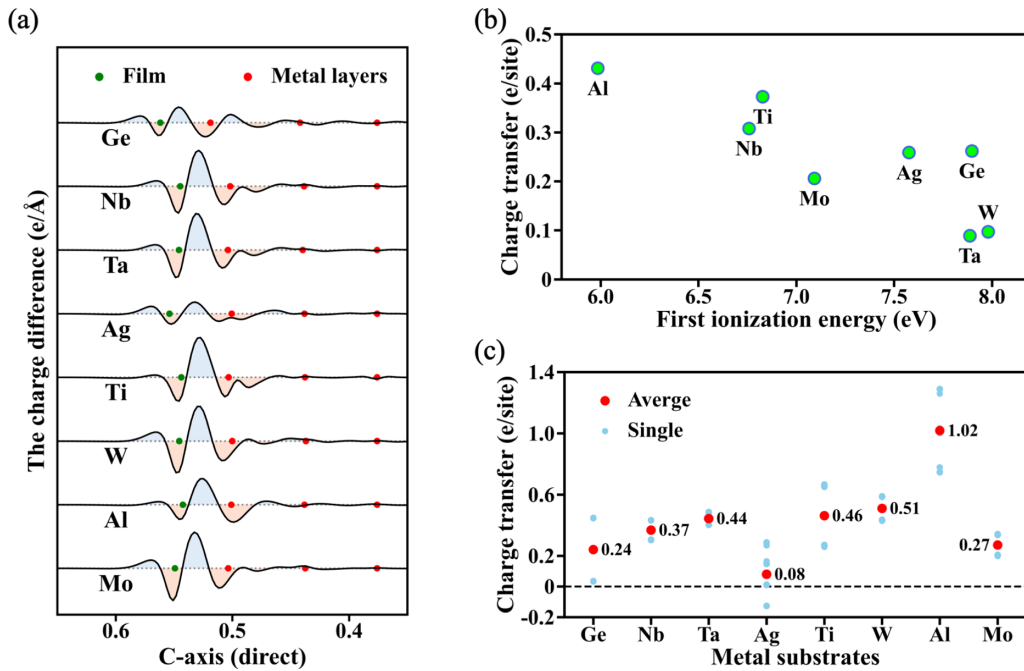
FIG. 3. The variation of charge density along the c direction and charge transfer. (a) The variation of charge density along the c axis. The ticks of the c axis are expressed in direct coordinates. The light blue (orange) region corresponds to the increase (decrease) in charge density. (b) The charge transfer obtained by integrating the charge difference curve obtained for (a) along the c axis ranges from the vacuum to the peak of the charge difference between the film and the substrate, as a function of the first ionization energy of metals, shown as a negative correlation. (c) The Bader charge analysis. The red (light blue) dots represent the average (individual) number of electrons gained by boron atoms.

energy, the more stable the film is, and vice versa. Figure 2(d) demonstrates that, for all metals, the hollow sites are energetically preferred comparing to top sites. Generally speaking, the E_{ad} of the hollow sites is $0.65 \sim 2.17$ eV per site, larger than that of the top sites, and differences $[\Delta E_{ad} = E_{ad}(hollow) - E_{ad}(top)]$ are 0.22, 0.27, 0.37, 0.08, 0.42, 0.16, 0.26, and 0.20 eV per site for Ge, Nb, Ta, Ag, Ti, W, Al, and Mo, respectively. For Ag substrate, the E_{ad} of the hollow sites is 0.08 eV per site higher than that of the top sites, suggesting that the h-B may also be grown at the top sites mediated by thermal energy, strain, or other types of perturbation. Since the hollow sites are more stable for all metal substrates, the adhesive energy denotes the adhesive energy of the hollow sites throughout the paper, otherwise stated.

Our result presents that the E_{ad} are 0.85, 2.00, 2.17, 0.65, 1.93, 2.06, 1.13, and 1.97 eV per site for Ge, Nb, Ta, Ag, Ti, W, Al, and Mo, respectively. Previously, the h-B has been experimentally synthesized on Al substrate by Li *et al.* [28]. The E_{ad} on Al substrate from our DFT calculation is in good agreement with the results from Zhang *et al.* [27] (1.10 eV per site), but larger than the values reported by Zhu *et al.* [36] as they overlooked the van der Waals interaction in their calculations. One would assume that the larger the E_{ad}, the more stable the h-B is. Hence, the Nb, Ta, Ti, W, and Mo substrates in the fcc phase may serve as a better substrate than Al to support the h-B growth as the E_{ad} are 2.00, 2.17, 1.93, 2.06, and 1.97 eV per site for Nb, Ta, Ti, W, and Mo, respectively. The E_{ad} of Ag, which is 0.65 eV per site, is consistent with Zhang *et al.* (0.63 eV per site) [27], too small

to stabilize the h-B; hence, the Ag substrate does not work experimentally towards fabricating h-B.

The ground-state electron configuration of boron is $[He]2s^2 2p^1$, one electron less than the carbon atom. If an extra electron is added to the h-B to form a π bond, the boron should behave just like the carbon; hence, the h-B becomes thermodynamically stable. From the DFT calculation, we can extract the charge-transfer effect between the substrate and film as the charge-transfer effect is a good indicator for searching for a viable substrate.

Figure 3(a) gives the variation of charge density along the c axis when attaching h-B onto the substrate. As the h-B grows on the substrate, the charge transfer occurs mainly within the film and the surface metal layer of the substrate, and the charge mainly accumulates toward the interlayer between the two. The Nb, Ta, Ti, W, and Mo substrate in the fcc phase can supply sufficient change transfer, comparable to the Al substrate, to electronically dope and stabilize the h-B. On the Ag and Ge substrate, the charge transfer from the metal to h-B is small, implying the weak and unstable film-substrate coupling. It can be concluded from the data that the amount of charge transfer is proportional to the adhesive energy.

To quantitatively evaluate the charge-transfer effect, the charge difference curve is integrated for the h-B along the c axis ranging from the vacuum to the peak of the charge difference between the film and substrate [Fig. 3(b)]. The integration of the charge-transferring curve shows the number of electrons that were transferred from the metal substrate to the h-B. We found that the charge-transfer effect is linearly correlated with the first ionization energy of the metal. The
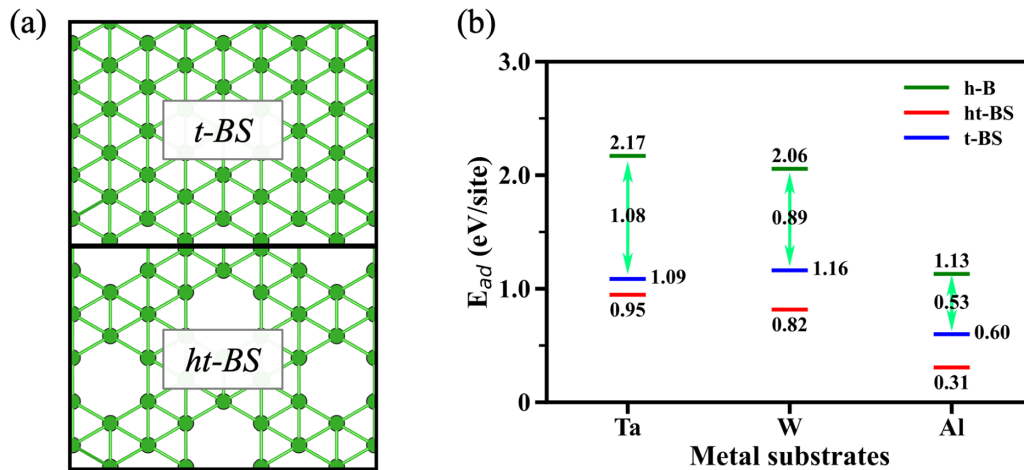
FIG. 4. Schematic structures of two other types of BSs and their E_{ad} on Ta, W, and Al substrates. (a) The t-BS and ht-BS from top to bottom, respectively. (b) The E_{ad} of three types of BSs grown on Ta, W, and Al substrates. The h-B on fcc Al, Ta, and W substrates thermodynamically outcompetes other phases of BSs as the E_{ad} of t-BS/substrate and ht-BS/substrate are smaller. The E_{ad} difference between h-B and t-BS also confirms that Ta and W are superior to Al for h-B growth.

first ionization energy, as the name implies, is the energy required for an elemental atom to lose its first outermost electron. The higher the first ionization energy, the more difficult it is for an atom to lose one electron. The linear trend in the figure corresponds to just this negative correlation. Al, which has the smallest first ionization energy, is likely to lose the most electrons; whereas the W and Ta, on the other side of the chart, prefer to offer less excessive charge as they have larger first ionization energy. We also found that h-B gains on average ∼1.02 electrons per atom when contacted with Al substrate according to the Bader charge analysis [38] [Fig. 3(c)], in line with the 1.05 electrons per atom obtained by Zhu *et al.* [36]. We infer that the first ionization energy can be utilized as useful guidance to estimate the charge transfer.

Considering the adhesive energy, charge transfer, and other metrics, it implies that Ta and W are the two most likely substrates. We carried out first-principles molecular-dynamics calculations at 300 K for h-B on Ta and W (see Fig. S1 in the Supplemental Material [39]), respectively. The results show that the h-B retains its structure under 300 K; hence these structures are dynamically stable at room temperature.

The growth of h-B may compete with a couple of BS allotropes, such as the t-BS and ht-BS as shown in Fig. 4(a). Based on our calculation, it has been confirmed that the h-B on fcc Al, Ta, and W substrates thermodynamically outcompetes other phases of BSs (i.e., t-BS and ht-BS) by 1.08, 0.89, and 0.53 eV per site, respectively [Fig. 4(b)].

The most stable phase of the eight metals (e.g., Ta and W) in nature is either body-centered cubic (bcc) or hexagonal close packed (hcp). So, can their fcc phases be made? Existing literature (Table I) hints that they all can have the fcc phase under certain circumstances. Denbigh and Marcus [40] grew fcc films of Mo and Ta on carbon, silicon oxide, and magnesium oxide by evaporation or vapor-phase epitaxy (VPE). Chopra *et al.* [41] achieved the growth of the fcc films of Ta, Mo, and W on rocksalt by vacuum sputtering. Marcus and Quigley [42] also observed fcc films of Ta by

electron-beam evaporation. In recent years, Shiri *et al.* [43] obtained thin films of fcc Ta successfully by deposition on silicon using magnetron sputtering (MS). The lattice parameters of Ta films given by them are 4.40 Å [40], 4.39 Å [41], 4.42 Å [42], and 4.51 Å [43], respectively, with an offset of nearly 0.1 Å.

Regarding the thin-film growth for the fcc Ti, the presence of the fcc Ti was observed by Shechtman *et al.* [44] through deposition on glass substrates employing electron beam guns in a cryopumped vacuum chamber. Saleh *et al.* [45,46] subsequently grew thin films of fcc Ti by epitaxial growth with Al as the substrate. Chakraborty *et al.* [47], Arshi *et al.* [48], and Fazio *et al.* [49] grow Ti fcc films on silicon by direct current magnetron sputtering (DCMS)/electron beam/vacuum arc discharge, indicating that silicon is a good substrate for growing fcc metals, respectively. Their measured lattice constants for fcc Ti are 4.42 Å [44], 4.22 Å [45], 4.20 Å [46], 4.16 Å [47], 4.05 Å [48], and 4.20 Å [49], with offsets of roughly 0.1 Å, except for a few cases. Sasaki *et al.* [50] prepared Nb films with fcc phase on ultrasonically vibrated substrates using halide chemical vapor deposition (HCVD). Kacim *et al.* [51] prepared fcc Mo films with impurities on sintered polycrystalline MgO by deposition. The corresponding lattice parameters are summarized in Table I. Among these lattice constants obtained from experiments, only the lattice constant of Ta is slightly different from the one used in the calculations. In this respect, we performed the same calculations using the experimental lattice constant 4.40 Å for the fcc phase of Ta and obtained the same conclusion as those using the ideal lattice parameters.

Hence, we predict that the h-B can be fabricated on several other metal substrates other than Al. The trick is to first make the metal film into the fcc phase. The metastable substrate of Nb, Ta, Ti, W, and Mo, in the fcc phase, can bind h-B tightly even better than the Al by 1.04 eV per site. Stability-wise, there is an interplay between the substrate and the film, and slight shaking on the stability on the substrate side can lead to improved stabilization on the film side. The π bands

TABLE I. Some research works about fcc film growth for the metals Nb, Ta, Ti, W, and Mo.

Metal	E_{hull} (eV)	a_0 (Å)	Possible substrate	Method	Reference
Nb	0.342	3.96	Ultrasound-vibrating substrates	HCVD	[50]
		4.23	Silicon	DCMS	[52]
Ta	0.246	4.40	Carbon, SiO_2, MgO	Evaporation/VPE	[40]
		4.39	Rocksalt	Vacuum sputtering	[41]
		4.42	MgO	Evaporation	[42]
		4.51	Silicon	Magnetron sputtering	[43]
Ti	0.063	4.42	Glass	Electron beam	[44]
		4.22	Al	Epitaxial growth	[45]
		4.20	Al	Epitaxial growth	[46]
		4.16	Silicon	DCMS	[47]
		4.05	Silicon/SiO_2	Electron beam	[48]
		4.20	Silicon	Vacuum arc discharge	[49]
W	0.480	4.15	Glass, rocksalt, mica	Sputtering	[53]
		4.13	Rocksalt	Vacuum sputtering	[41]
Mo	0.428	4.19	Rocksalt	Vacuum sputtering	[41]
		4.18	MgO	Evaporation/sputtering	[51]

E_{hull}: energy above hull, the energy of decomposition of one material into the set of most stable materials at this chemical composition, in eV per atom. 0 eV per atom means this material is the most stable. a_0: lattice parameter.

of h-B are strongly hybridized with substrates and the band structure is deformed in these cases (see Fig. S2 [39]). Thus, it is expected that the h-B on those substrates have different transport properties from freestanding ones.

IV. CONCLUSION

In summary, via *ab initio* calculations, we studied the structure, energy, and electronic stability of the h-B growth on fcc Ge, Nb, Ta, Ag, Ti, W, Al, and Mo(111). Flatness, interlayer coupling distance, and adhesive energy have been evaluated for the h-B. It is evident that hollow sites are superior to top sites for the accommodation of h-B. Moreover, with fcc Nb, Ta, Ti, W, and Mo as substrates, a better structural characterization than Al is obtained, namely, the h-B on these substrates could be flatter with a larger layer spacing and adhesive energy (at least 0.80 eV per atom) stronger than on Al. Following the analysis of charge-transfer effects, we found not only a more robust interlayer coupling strength than Al for Nb, Ta, Ti, W, and Mo, but also the negative correlation between the number of electrons gained and the first ionization energy of the substrate after integrating the charge-transfer curves. Also,

the agreement of Bader charge analysis with the literature justifies our results, for example, for Al, $\sim$1.02 electron/site. Among them, Ta is an optimal choice, followed by W. Their larger adhesive energy keeps h-B more stable and almost no charge transfer is required. Although the most stable phase of these metals in nature is either bcc or hcp, these metals are metastable and have been experimentally prepared in the fcc phase. We conclude that a variety of metal thin films can be used as optimal substrates for the growth of h-B growth with additional advantages of being easier to grow pure h-B that is more stable and flatter. If the h-B can be made on Ta, and W, a worthwhile direction is to study the superconductivity with the h-B. As it is exposed on the surface, it provides an extra dimension for people to engineer/measure its properties.

ACKNOWLEDGMENTS

[1] K. S. Novoselov, A. K. Geim, S. V. Morozov, D. Jiang, M. I. Katsnelson, I. V. Grigorieva, S. V. Dubonos, and A. A. Firsov, Two-dimensional gas of massless Dirac fermions in graphene, Nature (London) **438**, 197 (2005).

[2] K. S. Novoselov, Z. Jiang, Y. Zhang, S. V. Morozov, H. L. Stormer, U. Zeitler, J. C. Maan, G. S. Boebinger, P. Kim, and A. K. Geim, Room-temperature quantum Hall effect in graphene, Science **315**, 1379 (2007).

[3] C. L. Kane and E. J. Mele, Quantum Spin Hall Effect in Graphene, Phys. Rev. Lett. **95**, 226801 (2005).

[4] C. L. Kane and E. J. Mele, Z2 Topological Order and the Quantum Spin Hall Effect, Phys. Rev. Lett. **95**, 146802 (2005).

[5] D. N. Sheng, Z. Y. Weng, L. Sheng, and F. D. Haldane, Quantum Spin-Hall Effect and Topologically Invariant Chern Numbers, Phys. Rev. Lett. **97**, 036808 (2006).

[6] C. C. Liu, W. Feng, and Y. Yao, Quantum Spin Hall Effect in Silicene and Two-Dimensional Germanium, Phys. Rev. Lett. **107**, 076802 (2011).

[7] C.-L. Lin, R. Arafune, K. Kawahara, M. Kanno, N. Tsukahara, E. Minamitani, Y. Kim, M. Kawai, and N. Takagi, Substrate-Induced Symmetry Breaking in Silicene, Phys. Rev. Lett. **110**, 076801 (2013).

[8] Z. Qiao, S. A. Yang, W. Feng, W.-K. Tse, J. Ding, Y. Yao, J. Wang, and Q. Niu, Quantum anomalous Hall effect in graphene

from Rashba and exchange effects, Phys. Rev. B **82**, 161414(R) (2010).

[9] G.-F. Zhang, Y. Li, and C. Wu, Honeycomb lattice with multiorbital structure: Topological and quantum anomalous Hall insulators with large gaps, Phys. Rev. B **90**, 075114 (2014).

[10] J. Kortus, I. I. Mazin, K. D. Belashchenko, V. P. Antropov, and L. L. Boyer, Superconductivity of Metallic Boron in MgB$_2$, Phys. Rev. Lett. **86**, 4656 (2001).

[11] M. Gao, Z.-Y. Lu, and T. Xiang, Prediction of phonon-mediated high-temperature superconductivity in Li$_3$B$_4$C$_2$, Phys. Rev. B **91**, 045132 (2015).

[12] M. Xu, T. Liang, M. Shi, and H. Chen, Graphene-like two-dimensional materials, Chem. Rev. **113**, 3766 (2013).

[13] H. Tang and S. Ismail-Beigi, Novel Precursors for Boron Nanotubes: The Competition of Two-Center and Three-Center Bonding in Boron Sheets, Phys. Rev. Lett. **99**, 115501 (2007).

[14] K. C. Lau and R. Pandey, Stability and electronic properties of atomistically-engineered 2D boron sheets, J. Phys. Chem. C **111**, 2906 (2007).

[15] X.-F. Zhou, X. Dong, A. R. Oganov, Q. Zhu, Y. Tian, and H.-T. Wang, Semimetallic Two-Dimensional Boron Allotrope with Massless Dirac Fermions, Phys. Rev. Lett. **112**, 085502 (2014).

[16] B. Aufray, A. Kara, S. Vizzini, H. Oughaddou, C. Léandri, B. Ealet, and G. Le Lay, Graphene-like silicon nanoribbons on Ag(110): A possible formation of silicene, Appl. Phys. Lett. **96**, 183102 (2010).

[17] B. Lalmi, H. Oughaddou, H. Enriquez, A. Kara, S. Vizzini, B. Ealet, and B. Aufray, Epitaxial growth of a silicene sheet, Appl. Phys. Lett. **97**, 223109 (2010).

[18] P. Vogt, P. De Padova, C. Quaresima, J. Avila, E. Frantzeskakis, M. C. Asensio, A. Resta, B. Ealet, and G. Le Lay, Silicene: Compelling Experimental Evidence For Graphenelike Two-Dimensional Silicon, Phys. Rev. Lett. **108**, 155501 (2012).

[19] L. Li, S.-Z. Lu, J. Pan, Z. Qin, Y.-Q. Wang, Y. Wang, G.-Y. Cao, S. Du, and H.-J. Gao, Buckled germanene formation on Pt(111), Adv. Mater. **26**, 4820 (2014).

[20] N. Gonzalez Szwacki, A. Sadrzadeh, and B. I. Yakobson, B80 Fullerene: An Ab Initio Prediction of Geometry, Stability, and Electronic Structure, Phys. Rev. Lett. **98**, 166804 (2007).

[21] H.-J. Zhai, Y.-F. Zhao, W.-L. Li, Q. Chen, H. Bai, H.-S. Hu, Z. A. Piazza, W.-J. Tian, H.-G. Lu, Y.-B. Wu, Y.-W. Mu, G.-F. Wei, Z.-P. Liu, J. Li, S.-D. Li, and L.-S. Wang, Observation of an all-boron fullerene, Nat. Chem. **6**, 727 (2014).

[22] M. H. Evans, J. D. Joannopoulos, and S. T. Pantelides, Electronic and mechanical properties of planar and tubular boron structures, Phys. Rev. B **72**, 045434 (2005).

[23] B. Feng, J. Zhang, Q. Zhong, W. Li, S. Li, H. Li, P. Cheng, S. Meng, L. Chen, and K. Wu, Experimental realization of two-dimensional boron sheets, Nat. Chem. **8**, 563 (2016).

[24] X. Sun, X. Liu, J. Yin, J. Yu, Y. Li, Y. Hang, X. Zhou, M. Yu, J. Li, G. Tai, and W. Guo, Two-dimensional boron crystals: Structural stability, tunable properties, fabrications and applications, Adv. Funct. Mater. **27**, 1603300 (2017).

[25] Y. Liu, E. S. Penev, and B. I. Yakobson, Probing the synthesis of two-dimensional boron by first-principles computations, Angew. Chem. Int. Ed. **52**, 3156 (2013).

[26] H. Liu, J. Gao, and J. Zhao, From boron cluster to two-dimensional boron sheet on Cu(111) surface: Growth mechanism and hole formation, Sci. Rep. **3**, 3238 (2013).

[27] L. Z. Zhang, Q. B. Yan, S. X. Du, G. Su, and H. J. Gao, Boron sheet adsorbed on metal surfaces: Structures and electronic properties, J. Phys. Chem. C **116**, 18202 (2012).

[28] W. Li, L. Kong, C. Chen, J. Gou, S. Sheng, W. Zhang, H. Li, L. Chen, P. Cheng, and K. Wu, Experimental realization of honeycomb borophene, Sci. Bull. **63**, 282 (2018).

[29] G. Kresse and J. Furthmüller, Efficient iterative schemes for ab initio total-energy calculations using a plane-wave basis set, Phys. Rev. B **54**, 11169 (1996).

[30] J. P. Perdew, K. Burke, and M. Ernzerhof, Generalized Gradient Approximation Made Simple, Phys. Rev. Lett. **77**, 3865 (1996).

[31] G. Kresse and D. Joubert, From ultrasoft pseudopotentials to the projector augmented-wave method, Phys. Rev. B **59**, 1758 (1999).

[32] S. Grimme, J. Antony, S. Ehrlich, and H. Krieg, A consistent and accurate ab initio parametrization of density functional dispersion correction (DFT-D) for the 94 elements H-Pu, J. Chem. Phys. **132**, 154104 (2010).

[33] S. Grimme, S. Ehrlich, and L. Goerigk, Effect of the damping function in dispersion corrected density functional theory, J. Comput. Chem. **32**, 1456 (2011).

[34] J. Neugebauer and M. Scheffler, Adsorbate-substrate and adsorbate-adsorbate interactions of Na and K adlayers on Al(111), Phys. Rev. B **46**, 16067 (1992).

[35] A. J. Mannix, X.-F. Zhou, B. Kiraly, J. D. Wood, D. Alducin, B. D. Myers, X. Liu, B. L. Fisher, U. Santiago, J. R. Guest, M. J. Yacaman, A. Ponce, A. R. Oganov, M. C. Hersam, and N. P. Guisinger, Synthesis of borophenes: Anisotropic, two-dimensional boron polymorphs, Science **350**, 1513 (2015).

[36] L. Zhu, B. Zhao, T. Zhang, G. Chen, and S. A. Yang, How is honeycomb borophene stabilized on Al(111)?, J. Phys. Chem. C **123**, 14858 (2019).

[37] I. Boustani, A. Quandt, E. Hernández, and A. Rubio, New boron based nanostructured materials, J. Phys. Chem. C **110**, 3176 (1999).

[38] E. Sanville, S. D. Kenny, R. Smith, and G. Henkelman, Improved grid-based algorithm for Bader charge allocation, J. Comput. Chem. **28**, 899 (2007).

[39] See Supplemental Material at http://link.aps.org/supplemental/10.1103/PhysRevMaterials.5.104003 for molecular-dynamics simulation and electronic structure.

[40] P. N. Denbigh and R. B. Marcus, Structure of very thin tantalum and molybdenum films, J. Appl. Phys. **37**, 4325 (1966).

[41] K. L. Chopra, M. R. Randlett, and R. H. Duff, Face-centred cubic modification in sputtered films of tantalum, molybdenum, tungsten, rhenium, hafnium and zirconium, Philos. Mag. **16**, 261 (1967).

[42] R. B. Marcus and S. Quigley, Formation of f.c.c., b.c.c. and β-tantalum films by evaporation, Thin Solid Films **2**, 467 (1968).

[43] S. Shiri, A. Odeshi, N. Chen, R. Feng, R. Sutarto, and Q. Yang, FCC tantalum thin films deposited by magnetron sputtering, Surf. Coat. Technol. **358**, 942 (2019).

[44] D. Shechtman, D. Van Heerden, and D. Josell, fcc titanium in Ti-Al multilayers, Mater. Lett. **20**, 329 (1994).

[45] A. A. Saleh, V. V. Shutthanandan, and R. J. Smith, Observation of ultrathin metastable fcc Ti films on Al(110) surfaces, Phys. Rev. B **49**, 4908 (1994).

[46] A. A. Saleh, V. Shutthanandan, N. R. Shivaparan, R. J. Smith, T. T. Tran, and S. A. Chambers, Epitaxial growth of fcc Ti films on Al(001) surfaces, Phys. Rev. B **56**, 9841 (1997).

[47] J. Chakraborty, K. Kumar, R. Ranjan, S. G. Chowdhury, and S. R. Singh, Thickness-dependent fcc–hcp phase transformation in polycrystalline titanium thin films, Acta Mater. **59**, 2615 (2011).

[48] N. Arshi, J. Lu, C. G. Lee, J. H. Yoon, B. H. Koo, and F. Ahmed, Thickness effect on properties of titanium film deposited by d.c. magnetron sputtering and electron beam evaporation techniques, Bull. Mater. Sci. **36**, 807 (2013).

[49] M. Fazio, D. Vega, A. Kleiman, D. Colombo, L. M. Franco Arias, and A. Márquez, Study of the structure of titanium thin films deposited with a vacuum arc as a function of the thickness, Thin Solid Films **593**, 110 (2015).

[50] M. Sasaki, M. Koyano, H. Negishi, and M. Inoue, F.c.c. niobium films grown by halide chemical vapour deposition on ultrasound-vibrating substrates, Thin Solid Films **158**, 123 (1988).

[51] S. Kacim, P. Delcambe, L. Binst, M. Jardinier-Offergeld, and F. Bouillon, Structural behavior of direct-current sputtered and thermally evaporated molybdenum thin films, Thin Solid Films **249**, 150 (1994).

[52] J. Y. Zhang, P. Zhang, X. Zhang, R. H. Wang, G. Liu, G. J. Zhang, and J. Sun, Mechanical properties of fcc/fcc Cu/Nb nanostructured multilayers, Mater. Sci. Eng. A **545**, 118 (2012).

[53] K. L. Chopra, M. R. Randlett, and R. H. Duff, Face-centered-cubic Tungsten films obtained by, Appl. Phys. Lett. **9**, 402 (1966).